


**DEVELOPMENT OF BILAYER TiO₂ PHOTOCATALYST SYSTEMS
IMMOBILIZED ON STAINLESS STEEL PLATE AND THEIR PHYSICAL AND
PHOTOCATALYTIC CHARACTERIZATION**

by

CHONG KIAN WEI



**Thesis submitted in fulfilment of the
requirements for the degree of
Doctor of Philosophy**

May 2007

ACKNOWLEDGEMENTS

I would like to express my gratitude to all those who gave me the support to complete this thesis. I want to thank the former Dean of School of Chemical Sciences for giving me the permission to commence work for this thesis in the first instance, to do the necessary research work and to use the school facilities.

I am deeply indebted to my supervisor Prof. Dr. Mohd. Asri bin Mohd. Nawi from the School of Chemical Sciences whose help, stimulating suggestions and encouragement helped me during the research for writing this thesis.

I would like to convey my thanks to all the staff of the School of Chemical Sciences and School of Biological Sciences, who had supported and assisted me throughout my research in USM especially the handling of various types of analytical equipment.

I would like to pass along my very special thanks to my parents for their patience, continuous blessings and support during the time I was far away from them.

Lastly, I would like to take this opportunity to thank Universiti Sains Malaysia for financially supporting me under the Graduate Assistant Scheme throughout my three years research. Finally, I also would like to thank the Malaysian Government for supporting and financing this project under FRGS Grant, No: 305/pkimia/610806.

TABLE OF CONTENTS

	Page
ACKNOWLEDGEMENTS	ii
TABLE OF CONTENTS	iii
REFERENCES	xiii
LIST OF TABLES	xiv
LIST OF FIGURES	xvi
LIST OF ABBREVIATION	xxii
LIST OF APPENDICES	xxiii
LIST OF PUBLICATION & SEMINAR	xxiv
ABSTRAK	xxv
ABSTRACT	xxviii
 CHAPTER ONE: INTRODUCTION AND LITERATURE REVIEW	
1 Introduction	1
1.1 Basic principles of heterogeneous photocatalysis	7
1.2 Mechanism of the Photocatalytic Reaction	11
1.3 Role of adsorption in photocatalytic degradation	21
1.4 Dopants/coupled semiconductor	34
1.5 Nickel oxide and its applications	47
1.6 Chitosan	49
1.7 Application of Chitosan in wastewater treatment	51
1.8 Scope and objective of this research	58
1.8.1 Problem statement	58
1.8.2 Overall outline plan of this research	59
1.8.3 Objectives of research	61
 CHAPTER TWO: EXPERIMENTAL AND METHODOLOGY	
2.0 EXPERIMENTAL	63

2.1	Chemicals and Equipments	63
2.2	Standard preparation	64
2.2.1	CBR dye standard solution preparation	64
2.2.2	Methylene blue standard solution preparation	65
2.2.3	Bromocresol purple standard solution preparation	65
2.3	Experimental set up	65
2.3.1	UV irradiation	65
2.3.2	Visible light irradiation	66
2.4	Data manipulation	67
2.5	Screening experiments on the photocatalytic efficiency of TiO ₂ coupled with various metal oxides and metal sulfides for the degradation of cibacron brilliant red textile dye under UV illumination	68
2.5.1	The effect of the twelve metal oxide to the TiO ₂ photocatalytic activity through impregnation method	68
2.5.2	The effect of different metal oxides and metal sulfides bilayer systems immobilized via electrophoretic deposition method on the TiO ₂ photocatalytic activity	69
2.6	Characterization of NiO using TEM, XRD and BET	71
2.6.1	TEM	71
2.6.2	XRD	71
2.6.3	BET	71
2.6.3	EDX	72
2.7	First and second layers photocatalyst preparation	72
2.7.1	TiO ₂	72
2.7.2	NiO	72
2.8	Immobilized photocatalyst preparation	73
2.8.1	Support solid preparation	73
2.8.2	Suspension preparation	73
2.8.2.1	TiO ₂ suspension	73
2.8.2.2	NiO suspension	73

2.9	Fabrication of TiO ₂ /NiO bilayer photocatalyst plates	74
2.9.1	The effect of layer arrangement on the sustainability of the photocatalytic efficiency of the TiO ₂ /NiO bilayer in the degradation of CBR dye under UV illumination	74
2.9.2	The effect of the Phenol-Formaldehyde resin (PF) on the immobilization rate of NiO onto the stainless steel plate	75
2.9.3	The effect of the Phenol-Formaldehyde resin (PF) amount to the TiO ₂ /NiO photocatalytic activity	76
2.9.4	Evaluation of optimized NiO calcining temperature via photocatalytic degradation of CBR dye	76
2.9.5	The effect of the calcination time of NiO on the photocatalyst activity of TiO ₂ /NiO bilayer system	77
2.9.6	The effect of the amount of TiO ₂ photocatalyst and NiO on the photocatalytic activity of the TiO ₂ /NiO bilayer system under 500 W UV and 45 W visible light irradiations	77
2.9.6.1	Optimization of the amount of NiO within TiO ₂ /NiO bilayer system	77
2.9.6.2	Optimization of the amount of TiO ₂ within the TiO ₂ /NiO bilayer system	78
2.9.7	The effect of the amount of the TiO ₂ layer on the reproducibility of the photocatalytic activity of TiO ₂ /NiO bilayer system upon repeated usage	78
2.10	The effect of some parameters in the application of TiO ₂ /NiO bilayer photocatalyst in the degradation of CBR dye, a model textile dye pollutant	79
2.10.1	The effect of the initial pH of CBR dye solutions on the TiO ₂ /NiO bilayer photocatalytic efficiency	79
2.10.2	The effect of the aeration flow rate on the TiO ₂ /NiO bilayer photocatalytic efficiency	79
2.10.3	The effect of CBR dye concentration on the TiO ₂ /NiO bilayer photocatalytic efficiency	80
2.10.4	The effect of inorganic additives on the photocatalytic degradation of CBR dye by TiO ₂ /NiO bilayer	80
2.10.4.1	Sodium persulfate	80
2.10.4.2	Sodium persulfate	80
2.10.4.3	Potassium bromate	81
2.10.5	The effect of pH on the TiO ₂ /NiO photocatalytic activity in	81

the presence of additive

2.11	Reusability or sustainability of the TiO ₂ /NiO bilayer in the degradation of textile dye in the presence of inorganic additives	82
2.12	Regeneration of the TiO ₂ /NiO photocatalytic activity	83
2.12.1	The effect of Na ₂ S ₂ O ₈ concentration in the regeneration of bilayer photocatalyst system	83
2.12.2	Optimization of the time of regeneration of bilayer plate by Na ₂ S ₂ O ₈	83
2.12.3	Recyclability of the TiO ₂ /NiO after regeneration	84
2.13	The effect of the nickel cation leaching from NiO layer on the photocatalytic activity of TiO ₂ /NiO bilayer system	84
2.13.1	Monitoring of the nickel and iron (III) cations leaching from the TiO ₂ /NiO bilayer catalyst	84
2.13.2	Monitoring of the nickel cation and sulfate anion leaching from NiO produced using different calcining temperature	85
2.13.3	Correlation between leached Ni ²⁺ ions and bilayer photocatalytic activity	86
2.13.4	Leaching of nickel cation from NiO layer (400 °C) in the presence of oxidant additives during photocatalytic experiment	86
2.13.5	Leaching of nickel cation from NiO layer (600 °C) in the presence of oxidant additives and its effect on photocatalytic activity of bilayer system	87
2.13.6	The effect of initial pH of CBR dye solutions on the leaching of nickel cation during photocatalytic degradation process	87
2.13.7	Determination of the relationship between volume of Na ₂ S ₂ O ₈ , amount of the nickel cation leaching and photocatalytic activity of bilayer system	88
2.14	Pretreatment process for the reduction of Ni ²⁺ cation leaching from TiO ₂ /NiO bilayer system	88
2.14.1	Optimization of the pretreatment duration	89
2.14.2	Optimization of the pretreatment temperature	89
2.14.3	TiO ₂ /NiO photocatalytic activity after pretreatment	89
2.15	Evaluation of CBR mineralization during its photocatalytic degradation	90
2.15.1	COD test of CBR dye	90

2.16	Content of nitrate anion in the CBR dye solution	91
2.17	The effect of the nickel cation on the TiO ₂ /NiO bilayer photocatalytic activity	92
2.18	The effect of nickel cation on the TiO ₂ single layer photocatalytic activity	92
2.19	The effect of iron (III) cation on the photocatalytic degradation of CBR dye by TiO ₂ /NiO bilayer system	93
2.20	Application of TiO ₂ /NiO bilayer in the degradation of bromocresol purple	94
2.20.1	Decolorization of bromocresol purple by TiO ₂ /NiO in various pH condition	94
2.20.2	Decolorization of bromocresol purple by TiO ₂ /NiO with addition of H ₂ O ₂ in various pH condition	94
2.20.3	Decolorization of bromocresol purple by TiO ₂ /NiO with addition of various additives	95
2.20.4	Sustainability of TiO ₂ /NiO bilayer in the photocatalytic degradation of bromocresol purple	95
2.21	Application of TiO ₂ /NiO bilayer in the degradation of methylene blue dyes	95
2.21.1	Rate of the degradation of methylene blue by TiO ₂ /NiO bilayer plate	95
2.21.2	The effect of the initial pH values on the degradation rate of methylene blue by TiO ₂ /NiO bilayer	96
2.21.3	Recyclability of the TiO ₂ /NiO to the decolorization of methylene blue at pH 12 and with addition of NaBH ₄	96
2.21.4	The effect of additives to the decolorization of methylene blue by TiO ₂ /NiO in different pH condition	97
2.21.5	The effect of nickel and iron (III) cations on the photocatalytic decolorization of methylene blue by TiO ₂ /NiO bilayer	97
2.22	Bilayer system involving non-metallic adsorbent: TiO ₂ /Chitosan hybrid system	98
2.22.1	Coating of chitosan as the underlayer and its optimized amount	98
2.22.1.1	Preparation of chitosan gel	98
2.22.1.2	Preparation of the TiO ₂ suspension	98
2.22.1.3	Preparation of immobilized chitosan gel on the stainless steel	98

2.22.1.4	Optimization of chitosan amount	98
2.22.1.5	Optimization of TiO ₂ amount	99
2.22.2	The effect of the adsorbed CBR dye on the chitosan surface	99
2.22.3	The effect of CBR dye solution pH on the photocatalytic efficiency of TiO ₂ /Chitosan bilayer	100
2.22.4	The effect of CBR dye concentration on the photocatalytic efficiency of TiO ₂ /Chitosan bilayer	101
2.22.5	The effect of electron scavenger	101
2.22.5.1	Hydrogen peroxide	101
2.22.5.2	Sodium persulfate	101
2.22.6	Optimization of chitosan calcining temperature	102
2.22.7	The effect of the calcination time of chitosan at optimum temperature on the photocatalytic activity of TiO ₂ /Chitosan	102
2.22.8	Recyclability of the immobilized TiO ₂ /chitosan photocatalytic activity in the absence and presence of additives	103
2.22.9	Content of COD for the CBR sample after treated with TiO ₂ /chitosan photocatalyst under visible light irradiation	103
2.22.10	Decolorization of bromocresol purple by TiO ₂ /NiO under various pH conditions and with addition of additives	103
2.22.11	Recyclability of the photocatalytic decolorization of bromocresol purple by TiO ₂ /Chitosan	104
2.22.12	Decolorization of methylene blue by TiO ₂ /chitosan in various condition	104

CHAPTER THREE: RESULTS AND DISCUSSION

3.0	Results and discussion	105
3.1	Fabrication and characterization of TiO ₂ /NiO bilayer hybrid system	106
3.1.1	Fabrication of bilayer photocatalyst immobilized on stainless steel plate using electrophoretic deposition.	106
3.1.2	Screening experiments on the photocatalytic efficiency of TiO ₂ coupled with various metal oxides and metal sulfides for the degradation of cibacron red textile dye under UV light irradiation	107
3.1.3	Synthesis and characterization of NiO	113

3.1.3.1	TEM analysis of the particle size of NiO catalyst	113
3.1.3.2	XRD analysis of NiO powders	115
3.1.3.3	BET surface analysis of the NiO particles	117
3.1.3.4	EDX analysis of the NiO particles	119
3.1.4	Fabrication of TiO ₂ /NiO bilayer photocatalyst plates	121
3.1.4.1	The effect of layer arrangement on the sustainability of the photocatalytic efficiency of the TiO ₂ /NiO bilayer in the degradation of CBR dye under UV light irradiation	121
3.1.4.2	The effect of Phenol-Formaldehyde resin (PF) on the coating time of NiO onto the stainless steel plate	124
3.1.4.3	The effect of Phenol-Formaldehyde resin (PF) additive on the photocatalytic activity of TiO ₂ /NiO bilayer plates.	125
3.1.4.4	Evaluation of optimized NiO calcining temperature via photocatalytic degradation of CBR dye	127
3.1.4.5	The effect of the calcination time of NiO on the photocatalytic activity of TiO ₂ /NiO bilayer system	130
3.1.4.6	Optimization of the amount of NiO within TiO ₂ /NiO bilayer system	131
3.1.4.7	Optimization of the amount of TiO ₂ within the TiO ₂ /NiO bilayer system	133
3.1.4.8	The effect of the amount of the TiO ₂ layer on the reproducibility of the photocatalytic activity of TiO ₂ /NiO bilayer system upon repeated usage	134
3.2	The effect of some operating parameters in the application of TiO ₂ /NiO bilayer photocatalyst system in the degradation of CBR dye, a model textile dye pollutant	142
3.2.1	The effect of the initial pH of CBR dye solutions on the TiO ₂ /NiO bilayer photocatalytic efficiency	143
3.2.2	The effect of the aeration flow rate on the TiO ₂ /NiO bilayer photocatalytic efficiency	144
3.2.3	The effect of CBR dye concentration on the TiO ₂ /NiO bilayer photocatalytic efficiency	147

3.2.4	The effect of inorganic additives on the photocatalytic degradation of CBR dye by TiO ₂ /NiO bilayer.	149
3.2.5	The effect of pH on the TiO ₂ /NiO photocatalytic activity in the presence of additive	152
3.3	Reusability or Sustainability of the TiO ₂ /NiO bilayers in the degradation of textile dye in the presence of inorganic additives	153
3.3.1	Sustainability of the TiO ₂ /NiO in the presence of Na ₂ S ₂ O ₈	154
3.3.2	Sustainability of the TiO ₂ /NiO in the presence of H ₂ O ₂ additive	156
3.3.3	Sustainability of the TiO ₂ /NiO in the degradation of CBR dye under the presence of KBrO ₃ and initial pH 4	158
3.4	Regeneration of the TiO ₂ /NiO photocatalytic activity	160
3.4.1	The effect of Na ₂ S ₂ O ₈ concentration in the regeneration of bilayer photocatalyst system	162
3.4.2	Optimization of the time of regeneration of bilayer photocatalyst plate by Na ₂ S ₂ O ₈	163
3.4.3	Sustainability of the TiO ₂ /NiO after regeneration	164
3.5	The effect of the nickel cations leaching from NiO layer on the photocatalytic activity of bilayer system	165
3.5.1	Leaching of the nickel cation from the TiO ₂ /NiO catalyst	165
3.5.2	Correlation between leached Ni ²⁺ ions and bilayer photocatalytic activity	168
3.5.3	Leaching of nickel cation from NiO layer (400 °C) in the presence of oxidant additives during photocatalytic experiments	169
3.5.4	Leaching of nickel cation from NiO layer (600 °C) in the presence of oxidant additives and its effect on photocatalytic activity of bilayer system	174
3.5.5	The effect of initial pH of CBR dye solutions on the leaching of nickel cation during photocatalytic degradation process.	176
3.5.6	Determination of the relationship between volume of Na ₂ S ₂ O ₈ , amount of the nickel cation leaching and photocatalytic activity of bilayer system	177
3.6	Pretreatment process for the reduction of Ni ²⁺ cations leaching from TiO ₂ /NiO bilayer system	179
3.6.1	TiO ₂ /NiO photocatalytic activity after pretreatment	182
3.7	Evaluation of CBR mineralization during its photocatalytic degradation	184

	by TiO ₂ /NiO bilayer hybrids	
3.7.1	COD test of CBR dye	184
3.7.2	Content of nitrate anion in the CBR dye solution	186
3.8	The effect of metal ions in the photocatalytic efficiency of TiO ₂ /NiO bilayer hybrid system	187
3.8.1	The effect of the nickel cation on the TiO ₂ /NiO bilayer photocatalytic activity	187
3.8.2	The effect of nickel cations on the TiO ₂ single layer photocatalytic activity	190
3.8.3	The effect of iron (III) cation on the photocatalytic degradation of CBR dye by TiO ₂ /NiO bilayer system.	192
3.9	The effect of chemical charges of the water pollutants on the photocatalytic behaviour of TiO ₂ /NiO bilayer	195
3.9.1	Application of TiO ₂ /NiO bilayer in the degradation of bromocresol purple	196
3.9.1.1	The rate of photocatalytic degradation of bromocresol purple by TiO ₂ /NiO	196
3.9.1.2	Sustainability of TiO ₂ /NiO bilayers in the photocatalytic degradation of bromocresol purple	201
3.9.2	Application of TiO ₂ /NiO bilayer plate for Photocatalytic Degradation of methylene blue	202
3.9.2.1	Rate of the degradation of methylene blue by TiO ₂ /NiO bilayer plate	202
3.9.2.2	The effect of the initial pH values on the degradation rate of methylene blue by TiO ₂ /NiO bilayer	204
3.9.2.3	Recyclability of the TiO ₂ /NiO in the decolorization of methylene blue at pH 12 and with addition of NaBH ₄	206
3.9.2.4	Nickel and iron (III) cations leaching at pH 12 from TiO ₂ /NiO bilayer during its photocatalytic degradation of methylene blue with addition of NaBH ₄	208
3.9.2.5	The effect of additives on the photocatalytic degradation of methylene blue by TiO ₂ /NiO under different pH condition	209
3.9.2.6	The effect of nickel cation on the photocatalytic	211

	degradation of methylene blue by TiO ₂ /NiO	
	3.9.2.7 The effect of iron (III) cation on the photocatalytic degradation of methylene blue by TiO ₂ /NiO	213
3.10	Bilayer system involving organic adsorbent : TiO ₂ /chitosan hybrid system	215
3.10.1	Coating of chitosan as the underlayer and its optimized amount	216
3.10.2	Optimization of amount of TiO ₂ within the TiO ₂ /chitosan bilayer	219
3.10.3	Optimization of chitosan drying temperature	222
3.10.4	The effect of the drying time of chitosan at optimum temperature on the photocatalytic activity of TiO ₂ /chitosan bilayer system	224
3.10.5	The effect of the adsorbed CBR dye on the chitosan surface on the photocatalytic activity of TiO ₂ /chitosan bilayer system	226
3.10.6	The effect of pH on the photocatalytic activity of TiO ₂ /chitosan bilayer	230
3.10.7	The effect of CBR dye concentration	232
3.10.8	The effect of electron scavenger	234
	3.10.8.1 Hydrogen peroxide	234
	3.10.8.2 Sodium persulfate	236
3.10.9	Recyclability/reusability of the immobilized TiO ₂ /chitosan plate in the decolorization of CBR dye	237
3.10.10	COD values of the CBR sample solution after treatment with TiO ₂ /chitosan photocatalyst under visible light irradiation	240
3.10.11	Decolorization of bromocresol purple by TiO ₂ /chitosan in various pH condition and with addition of additives	242
3.10.12	Recyclability of the decolorization of bromocresol purple	244
3.10.13	Decolorization of methylene blue by TiO ₂ /chitosan in various condition	246
 CHAPTER FOUR: CONCLUSION		
4.0	Conclusion	247
4.1	TiO ₂ /NiO bilayer photocatalyst	247

4.2	TiO ₂ /chitosan bilayer	252
	REFERENCES	255
	APPENDICES	270
	LIST OF PUBLICATION & SEMINAR	321

LIST OF TABLES

		Page
Table 1.1	Bandgap energies of various semiconductors at pH = 0 and its corresponding threshold wavelength (Rajeshwar and Ibanez, 1997)	10
Table 1.2	Oxidation potentials of some oxidants (Legrini, et al., 1993)	19
Table 2.1	Chemicals that were used in the research project	63
Table 2.2	Equipments that were used in the research project	64
Table 2.3	List of the salts that were used for impregnating immobilized TiO ₂ stainless steel plates.	69
Table 2.4	Volume in μL of 0.1 M additives that had been added into the CBR dye solution	82
Table 2.5	Summary of the CBR sample conditions with the types of additive present.	82
Table 3.1	Particle size of the NiO that had been calcined at various temperatures.	114
Table 3.2	XRD peaks for NiO	116
Table 3.3	Beta and theta values of XRD peaks for NiO that had been calcined at various temperatures.	116
Table 3.4	The percentage of the detected elements on the surface of the NiO that had been calcined at various calcining temperatures.	119
Table 3.5	Slope and standard deviation of the ten times repeating first order constant value with different amount of TiO ₂ on the NiO surface	135
Table 3.6	Thickness of the optimum TiO ₂ /NiO stainless plate	136
Table 3.7	Percentage of the element on the bilayer photocatalyst surface as obtained from EDX analyses.	161
Table 3.8	Amount of sulfate and nickel ions leaching from the catalyst that was calcined at various temperatures.	167
Table 3.9	Nitrate ion content in the CBR dye solution after treated	186
Table 3.10	Amount of nickel cation in the CBR dye solutions after photocatalytic treatment with TiO ₂ /NiO bilayer system with initial doping of free Ni ²⁺ ions. All concentrations are in unit of mg/L.	190
Table 3.11	Iron (III) cation in the CBR dye solution after photocatalytic treatment	194
Table 3.12	The remaining amount of nickel cation in the dye solution before	212

and after the irradiation.

Table 3.13	The remaining amount of iron (III) cation in the dye solution before and after the irradiation.	214
Table 3.14	Comparison of the first order rate constant value (k value) between photocatalytic decolorization and the adsorption decolorization.	220
Table 3.15	Comparison between decolorization of bromocresol purple by TiO_2/NiO and $\text{TiO}_2/\text{chitosan}$ photocatalysts in various conditions.	243
Table 4.1	Summary of the first order constant values of the decolorization of CBR, bromocresol purple and methylene blue by TiO_2 , TiO_2/NiO and $\text{TiO}_2/\text{chitosan}$ bilayer system.	254

LIST OF FIGURES

		Page
Figure 1.1	Various wastewater treatment technologies in environmental engineering (Chen et al., 2000).	4
Figure 1.2	Illustration of the generation of electron hole pairs in a spherical semiconductor particle (Boer, 1990)	8
Figure 1.3	Valence and conductance band positions of semiconductors at pH = 0 (Suppan, 1994).	9
Figure 1.4	Positions of valence and conduction bands of TiO ₂ (anatase) and the reduction potentials of metallic ions of interest at different pH (Chen et al., 2000).	21
Figure 1.5	Schematic diagram representing the interaction between colloidal CdS and TiO ₂ semiconductor (Gopidas et al., 1990).	35
Figure 1.6	Interaction between SnO ₂ and TiO ₂ in the TiO ₂ capped SnO ₂	42
Figure 1.7	Comparison of Molecular Structure of Chitin (1), Chitosan (2) and Cellulose (3) (Knaul et al., 1998)	49
Figure 1.8	The chitosan production with deacetylation of chitin (Frantisek, 2001)	50
Figure 1.9	Chitosan preparation from chitin and chitosan solution in acidic solvent (Kimica Corporation, 2000)	51
Figure 2.1	UV irradiation experimental setup	66
Figure 2.2	45 W visible light irradiation experimental setup	67
Figure 2.3	45 W visible light irradiation experimental setup for COD test	91
Figure 3.1	Screening various types of metal oxides and metal sulfides	108
Figure 3.2	Screening of four metal oxides under 45 W visible light irradiation with aeration.	109
Figure 3.3	Average size of 300 particles of NiO produced from various calcining temperatures for NiCO ₃ .	115
Figure 3.4	Mean crystallite diameter of the NiO that had been calcined at various temperatures.	117
Figure 3.5	BET surface area of the NiO that had been calcined at various temperatures.	118
Figure 3.6	Percentage of major elements in the NiO catalyst obtained from various calcining temperatures of NiCO ₃ .	120
Figure 3.7	Recyclability of the decolorization of CBR dye by different	123

arrangement of TiO₂ and NiO

Figure 3.8	Adsorption of CBR dye by bilayer TiO ₂ /NiO and NiO/TiO ₂ and monolayer of NiO and TiO ₂ under dark condition without aeration.	123
Figure 3.9	The effect of the amount of Phenol-Formaldehyde resin (PF) to the deposition rate of NiO onto the stainless steel plate.	125
Figure 3.10	The effect Phenol-Formaldehyde resin (PF) additive on the first order rate constant in the decolorization of 15 ppm CBR dye by bilayer TiO ₂ /NiO photocatalyst immobilized onto stainless steel at 45 W visible light fluorescence lamp.	126
Figure 3.11	First order rate constant of decolorization of 15 ppm CBR dye by TiO ₂ /NiO bilayer with NiO prepared at various calcining temperatures.	129
Figure 3.12	The effect of calcination time at 400 °C on the photocatalytic efficiency of TiO ₂ /NiO bilayer photocatalyst system based on the first order rate constant on the photocatalytic removal of 15 ppm CBR dye.	130
Figure 3.13	Optimization of the amount of NiO behind TiO ₂ under UV and visible light irradiations.	133
Figure 3.14	Optimization of TiO ₂ on the surface of NiO	134
Figure 3.15	The effect of TiO ₂ thickness to the TiO ₂ /NiO first order constant value to the decolorization of CBR dye solution. NiO amount was fixed to around 0.2 g.	137
Figure 3.16	Slope of the 10 times repeating of the different amount of TiO ₂ covering onto the NiO surface	138
Figure 3.17	NiO spot 1	138
Figure 3.18	NiO spot 2	139
Figure 3.19	NiO spot 3	139
Figure 3.20	NiO spot 4	140
Figure 3.21	TiO ₂ spot 1	140
Figure 3.22	TiO ₂ spot 2	141
Figure 3.23	TiO ₂ spot 3	141
Figure 3.24	TiO ₂ spot 4	142
Figure 3.25	The effect of the CBR dye solution pH to the first order constant value of the decolorization.	144
Figure 3.26	The effect of the aeration flow rate to the TiO ₂ /NiO first order	147

constant value of the decolorization of CBR dye.

Figure 3.27	First order rate constants for the decolorization of CBR dye solutions at various CBR initial concentrations using bilayer TiO ₂ /NiO system and 45 W visible light fluorescent lamp.	148
Figure 3.28	The effect of additives on the the first order rate constant value of 15 ppm CBR dye decolorization by photocatalysis using TiO ₂ /NiO bilayer system under 45 W visible light fluorescent lamp.	151
Figure 3.29	The effect of the CBR solution pH on the first order rate constant value of the photocatalytic decolorization by TiO ₂ /NiO bilayer under 45 W visible light irradiation of 15 ppm CBR dye solutions that had been added optimum volume of respective inorganic additives.	153
Figure 3.30	The effect of the Na ₂ S ₂ O ₈ amount to the recyclability of the CBR dye decolorization.	155
Figure 3.31	The effect of the H ₂ O ₂ amount to the sustainability of the CBR dye decolorization	157
Figure 3.32	Average first order constant for 10 repeating treatments of the various amount of H ₂ O ₂ added.	158
Figure 3.33	The effect of the dosage of KBrO ₃ on the sustainability of the CBR dye decolorization by TiO ₂ /NiO bilayer photocatalyst system	160
Figure 3.34	Optimization of the concentration of Na ₂ S ₂ O ₈ for the reactivation process	163
Figure 3.35	Optimization of the irradiation duration for the activation process	164
Figure 3.36	Recyclability of the TiO ₂ /NiO after regenerated from the activation process.	165
Figure 3.37	Amount of nickel and iron cations leaching from the TiO ₂ /NiO during the decolorization of CBR dye solution when irradiated by UV and visible light	166
Figure 3.38	Amount of nickel cation leaching and photocatalytic activity of the TiO ₂ /NiO catalyst, which was prepared from nickel oxide that had been calcined at various temperatures	169
Figure 3.39	Ni ²⁺ cation leaching in CBR solution by pretreated TiO ₂ /NiO with addition of additives.	171
Figure 3.40	Recyclability of the decolorization of CBR dye solution by TiO ₂ /NiO with various additives	173
Figure 3.41	Nickel cation leaching from nickel oxide that had been calcined at 600 °C in various conditions	175

Figure 3.42	Photocatalytic activity in various conditions for the catalyst that was prepared from nickel oxide that had been calcined at 600 °C	176
Figure 3.43	Nickel cation leaching in different pH CBR solutions	177
Figure 3.44	Ni ²⁺ cation leaching in different amount of Na ₂ S ₂ O ₈	178
Figure 3.45	Photocatalytic activity in different amount of 0.1 M Na ₂ S ₂ O ₈	179
Figure 3.46	Nickel cation leaching after pretreatment with acid and warm water	180
Figure 3.47	Optimizing the pretreatment duration	181
Figure 3.48	Optimization of the warm water temperature in the pretreatment process	182
Figure 3.49	Recyclability of the TiO ₂ /NiO bilayer photocatalyst system that had undergone through pretreatment process prior to its use in the photocatalytic degradation of CBR dye.	183
Figure 3.50	COD content of the 15 ppm CBR dye solution after it has been photocatalyzed under 45 W visible light fluorescent lamp using TiO ₂ /NiO bilayer photocatalyst for up to twelve hours	185
Figure 3.51	The effect of the nickel cation to the TiO ₂ /NiO photocatalytic activity	188
Figure 3.52	The effect of the nickel cations on the TiO ₂ photocatalytic activity of CBR dye solution under 45 W visible light fluorescent lamp	191
Figure 3.53	The effect of the iron (III) cation on the TiO ₂ /NiO photocatalytic activity in the removal of CBR dye	193
Figure 3.54	Equilibrium bromocresol purple in acidic and alkaline medium.	195
Figure 3.55	Methylene blue molecular structure	195
Figure 3.56	Decolorization of bromocresol purple through irradiation and adsorption with the presence of TiO ₂ /NiO	198
Figure 3.57	Decolorization of bromocresol purple by TiO ₂ /NiO under visible light with addition of H ₂ O ₂ at various pH conditions	199
Figure 3.58	Decolorization of bromocresol purple by TiO ₂ /NiO with addition of various additive. H ₂ O ₂ and Na ₂ S ₂ O ₈ were added into the acidic bromocresol purple solution and NaBH ₄ was added into the basic bromocresol purple solution	200
Figure 3.59	Recyclability of the decolorization of bromocresol purple by TiO ₂ /NiO catalyst in acidic medium and with addition of Na ₂ S ₂ O ₈ under 45 W visible light fluorescent lamp irradiation.	202

Figure 3.60	Decolorization of the methylene blue by TiO ₂ /NiO in neutral condition.	203
Figure 3.61	Photocatalytic decolorization of 12.5 mg/L methylene blue under different pH medium by TiO ₂ /NiO bilayer plate under 45 W visible light fluorescent lamp irradiation.	205
Figure 3.62	Recyclability of the TiO ₂ /NiO in the decolorization of methylene blue at pH 12 and with addition of NaBH ₄	207
Figure 3.63	Nickel and iron (III) cations leaching at pH 12 and with addition of NaBH ₄ .	208
Figure 3.64	The effect of additives on the decolorization of 12.5 mg/L methylene blue by TiO ₂ /NiO bilayer photocatalyst plate under different pH conditions.	210
Figure 3.65	The effect of nickel cation on the decolorization of methylene blue by TiO ₂ /NiO bilayer photocatalyst.	212
Figure 3.66	The effect of iron (III) cation on the decolorization of 12.5 mg/L methylene blue by TiO ₂ /NiO bilayer photocatalyst.	214
Figure 3.67	Photograph of chitosan layer on stainless steel plate.	216
Figure 3.68	Photograph of TiO ₂ /chitosan layer on stainless steel	217
Figure 3.69	Optimization of chitosan amount with constant amount of TiO ₂ layer within the TiO ₂ /chitosan bilayer system.	218
Figure 3.70	Optimization of the TiO ₂ amount on the chitosan surface	221
Figure 3.71	Ratio of the photocatalysis to adsorption of the TiO ₂ /chitosan.	221
Figure 3.72	The effect of drying temperatures of chitosan on the first order rate constant value of CBR dye removal under dark condition by immobilized TiO ₂ /chitosan bilayer.	223
Figure 3.73	The effect of the drying time of the chitosan on the first order rate constant value of the photocatalytic degradation of CBR dye by TiO ₂ /chitosan bilayer system.	225
Figure 3.74	pH of the CBR dye solution after one hour treatment by TiO ₂ /chitosan and also amount of catalyst that had been lost during the one hour treatment.	226
Figure 3.75	The effect of the adsorbed CBR dye to the TiO ₂ /chitosan photocatalytic activity.	228
Figure 3.76	Repeating adsorption of CBR dye onto the chitosan layer.	229
Figure 3.77	Repeating of the decolorization of CBR dye by TiO ₂ /CBR/chitosan system. All the repeating treatments, which had shown in Figure above, had been coated with a layer of TiO ₂ with exception to the first treatment.	229

Figure 3.78	The effect of the CBR dye solution pH to the first order constant value	231
Figure 3.79	The effect of the initial concentration of CBR dye solution on the first order rate constant value during photocatalytic degradation by TiO ₂ /chitosan bilayer system.	233
Figure 3.80	The effect of the added H ₂ O ₂ on the first order rate constant value during photocatalytic degradation by TiO ₂ /chitosan bilayer system.	235
Figure 3.81	The effect of Na ₂ S ₂ O ₈ addition to the first order constant value.	237
Figure 3.82	Recyclability decolorization of CBR dye using immobilized TiO ₂ /chitosan catalyst under visible light irradiation.	239
Figure 3.83	COD reading for the degradation of the CBR dye using immobilized TiO ₂ /chitosan catalyst.	241
Figure 3.84	Decolorization of bromocresol purple by TiO ₂ /chitosan in various pH condition and with addition of additives.	243
Figure 3.85	Recyclability of the bromocresol purple by TiO ₂ /chitosan catalyst.	245
Figure 3.86	Decolorization of methylene blue by TiO ₂ /chitosan catalyst.	246

LIST OF ABBREVIATION

AAS	Atomic Absorption Spectroscopy
COD	Chemical Oxygen Demand
g	Gram
mg	Milligram
min	Minute
mL	Milliliter
UV	Ultra Violet
μ L	Microlitre
rpm	Rotation per minute
ppm	Parts per million
CBR	Cibacron Brilliant Red
TEM	Transmission Electronic Microscopic
EDX	Energy Dispersion X-Ray
XRD	X-Ray Diffraction
BET	BET surface analysis

LIST OF APPENDICES

	Page
Appendix A	Image of the NiO particle size at various calcining temperatures (TEM scanning) 270
Appendix B	The results of XRD analysis for various calcining temperatures of NiO 273
Appendix C	The results of BET analysis for various calcining temperatures of NiO 279
Appendix D	EDX Spectrum and SEM image for the various calcining temperatures of NiO catalyst 285
Appendix E	Image of the NiO that had been calcined at 400 and 800 °C 303
Appendix F	EDX Spectrum for the carbon determination on the TiO ₂ /NiO bilayer catalyst surface 304
Appendix G	Polarographic Analysis Conditions and Spectrum for Sulfate Anion for various calcining temperatures of NiO 310
Appendix H	Polarographic Analysis Spectrum for Nitrate Anion 314
Appendix I	Image of the dye precipitation when coagulating with iron (III) in the study of effect of iron (III) cation in probing its effect on decolorization of the CBR dye by TiO ₂ /NiO bilayer catalyst under 45 W visible light irradiation 317
Appendix J	Critical Values of Correlation Coefficient, r 319
Appendix K	Image of the TiO ₂ /NiO bilayer catalyst that had been treated with methylene blue 320

LIST OF PUBLICATION & SEMINAR

	Page
1.1 Photocatalytic Decolorization Of CBR Dye Using Immobilized TiO_2 -NiO On Stainless Steel Plate	321

PEMBANGUNAN SISTEM FOTO-PEMANGKINAN TiO_2 DUA LAPISAN YANG DIPEGUN PADA KEPINGAN KELULI DAN PENCIRIAN SIFAT FIZIKAL DAN FOTO-PEMANGKINANNYA

ABSTRAK

Kelemahan utama TiO_2 ialah ia memerlukan cahaya UV di bawah 380 nm yang dianggap berbahaya kepada manusia and mahal dari segi kos untuk mengaktifkan sifat foto-pemangkinannya. Oleh sebab itu, pelbagai teknik telah digunakan untuk megubahkan aktiviti foto-pemangkinan TiO_2 . Salah satu kaedah ialah mendopkan atau menggabungkan pelbagai jenis logam oksida, logam sulfida, logam berat and ion logam kepada TiO_2 . Sejak kebelakangan ini, penjerap juga digunakan untuk mendop secara sampingan kepada TiO_2 . Dalam pengajian ini, lapisan TiO_2 dipegunkan pada permukaan lapisan penjerap NiO dan kitosan yang disokong pada kepingan keluli. Sistem ini dikenali sebagai sistem hibrid fotomangkin dua lapisan. Keberkesanan foto-pemangkinan sistem ini terhadap penyahwarnaan pencerup sibakron merah (CBR), metilena biru (MB) dan bromokresol ungu (BP) di bawah sinaran UV dan cahaya nampak telah dikajikan. Parameter-parameter untuk membina fotomangkin dua lapisan yang telah dioptimisasikan berdasarkan kepada keberkesanan foto-pemangkinannya terhadap penyahwarnaan penjerup CBR dalam pengajian ini ialah suhu pemanasan NiO dan suhu pengeringan kitosan dan jumlah resin fenol formaldehid, TiO_2 , NiO dan kitosan. Parameter-parameter lain yang telah dikajikan adalah kesan aditif-aditif tak organic dan kation logam yang terlarutlesap terhadap aktiviti foto-pemangkinan fotomangkin dua lapisan. Penjerap NiO yang telah dipanaskan dalam pelbagai suhu telah dicirikan dengan menggunakan TEM, EDX, XRD dan BET. Fotomangkin dua lapisan TiO_2/NiO boleh menyahwarnakan 90 dan 93.3 % penjerup CBR selepas disinarkan di bawah cahaya UV dan nampak selama satu jam. Ia juga boleh menyahwarnakan 34 % penjerup BP dalam media asid dan 96 % penjerup MB dalam media alkali selepas disinarkan selama satu jam di bawah cahaya nampak. Manakala,

fotomangkin dua lapisan TiO_2 /kitosan boleh menyahwarnakan 98 % penjerup BP, 87 % penjerup CBR dan kurang daripada 10 % penjerup MB di bawah sinaran cahaya nampak selama 30 minit. Suhu dan masa pemanasan optimum bagi NiO dan kitosan adalah 400 °C selama 10 jam dan 150 °C selama 5 jam. Jumlah optimum resin fenol formaldehid dalam penganapan penjerap NiO pada kepingan keluli adalah 0.05 g. Jumlah optimum TiO_2 dan NiO dalam fotomangkin dua lapisan TiO_2 /NiO adalah 0.07 g dan 0.2 g. Sementara, jumlah optimum bagi kedua-dua TiO_2 dan kitosan dalam fotomangkin dua lapisan TiO_2 /kitosan adalah 0.04 g masing-masing. Aditif-aditif agen pengoksidaan seperti H_2O_2 and $\text{Na}_2\text{S}_2\text{O}_8$ boleh meningkatkan kadar penyahwarnaan larutan penjerup CBR dan BP apabila ia digunakan bersama-sama dengan fotomangkin dua lapisan TiO_2 /NiO dan TiO_2 /kitosan. Di sebaliknya, aditif-aditif agen pengoksidaan membantutkan penyahwarnaan MB apabila ia digunakan bersama-sama dengan fotomangkin dua lapisan TiO_2 /NiO. Walau bagaimanapun, aditif agen penurunan seperti NaBH_4 meningkatkan penyahwarnaan penjerup MB apabila ia digunakan bersama-sama dengan fotomangkin dua lapisan TiO_2 /NiO. Fotomangkin dua lapisan melarutlesap 90 dan 35 ppm kation-kation nikel ke dalam larutan pencerup CBR untuk perawatan kali pertama apabila disinarkan di bawah cahaya UV dan nampak. Kation nikel yang terlarutlesap berkurang dalam perawatan seterusnya ke kurang daripada 10 ppm selepas perawatan ketiga untuk kedua-dua sistem sinaran UV dan nampak. Tiada kation ferum (III) yang terlarutlesap ke dalam larutan pencerup di bawah sinaran cahaya nampak. Kation nikel memangkinkan penyahwarnaan larutan pencerup CBR tetapi membantut penyahwarnaan pencerup MB apabila disinarkan di bawah cahaya nampak dengan kehadiran fotomangkin dua lapisan TiO_2 /NiO dan pengudaraan. Keputusan-keputusan TEM, XRD, EDX dan BET menunjukkan bahawa NiO yang dipanaskan pada suhu yang lebih tinggi mempunyai size zarah yang lebih besar. Akhirnya, activity foto-pemangkinan TiO_2 boleh ditingkatkan dengan penggandingan NiO dan kitosan sebagai lapisan kedua. Walau bagaimanapun, peningkatan ini kebanyakan untuk pencerup anionic. Kitosan meningkatkan aktiviti

foto-pemangkinan TiO_2 lebih daripada NiO . Ion nikel yang terlarulesap daripada penjerap NiO boleh memengaruhi aktiviti foto-pemangkinan TiO_2/NiO . Semua agen pengoksidaan meningkatkan penyahwarnaan penjerup anionik tetapi mengurangkan penyahwarnaan pencerup kationik. Kitosan adalah penjerap lebih sesuai dan baik berbanding dengan NiO kerana ia tidak melarutlesapkan sebarang pencemar yang beracun ke dalam larutan yang dirawat. Manakala, penjerap NiO membebaskan kation nikel ke dalam larutan yang dirawat dan langkah selanjutnya diperlukan untuk memindahkan kation nikel ini.

DEVELOPMENT OF BILAYER TiO₂ PHOTOCATALYST SYSTEMS IMMOBILIZED ON STAINLESS STEEL PLATE AND THEIR PHYSICAL AND PHOTOCATALYTIC CHARACTERIZATION

ABSTRACT

The main weakness of TiO₂ is that it needs UV light with wavelengths below 380 nm, which are considered hazardous to human being and expensive in term of cost, to activate its photocatalytic property. Therefore, various techniques had been used to improve the photocatalytic activity of TiO₂. One of the method was doping or combining various types of metal oxides, metal sulfides, noble metal or metal ion with TiO₂. Recently, adsorbent also had been used to co-doped with TiO₂. In this research, TiO₂ layer was immobilized onto the surface of NiO and chitosan adsorbents layer, which were supported onto stainless steel plate. This system was called bilayer photocatalyst hybrid system. Photocatalytic efficiencies of this system to the decolorization of cibacron brilliant red dye (CBR), methylene blue (MB) and bromocresol purple (BP) under UV and visible light illumination had been studied. Parameters of the fabrication of the bilayer photocatalyst that had been optimized based on its photocatalytic efficiency to the decolorization of CBR dye in this research were calcining temperatures of NiO and drying temperatures of chitosan and amount of phenol formaldehyde resin, TiO₂, NiO and chitosan. Other parameters that had been studied were effect of inorganic additives and metal cation leaching on the photocatalytic acitivity of the bilayer photocatalysts. NiO adsorbents that had been calcined at various temperatures were characterized using TEM, EDX, XRD and BET. TiO₂/NiO bilayer photocatalyst could decolorize 90 and 93.3 % of CBR dye after one-hour illumination under UV and visible light. It also could decolorize 34 % of BP dye in acidic medium and 96 % of MB dye in alkaline medium after one-hour illumination under visible light. Whereas, TiO₂/chitosan bilayer photocatalyst could decolorize 98 % of BP, 87 % of CBR and less than 10% of MB dyes under visible light illumination for

30 minutes. Optimum calcining temperature and duration for NiO and chitosan were 400 °C for 10 hours and 150 °C for 5 hours. Optimum amount of phenol formaldehyde resin in the deposition of NiO adsorbent onto stainless steel plate was 0.05 g. Optimum amounts of TiO₂ and NiO in the TiO₂/NiO bilayer photocatalyst were 0.07 g and 0.2 g. While, optimum amounts of both TiO₂ and chitosan in the TiO₂/chitosan bilayer photocatalyst were 0.04 g, respectively. Oxidant additives such as H₂O₂ and Na₂S₂O₈ could increase the decolorization rate of CBR and BP dye solution when it was utilized together with TiO₂/NiO and TiO₂/Chitosan bilayer photocatalysts. Contrary, oxidant additives retarded decolorization of MB when it was utilized together with TiO₂/NiO bilayer photocatalyst. However, reductant additive such as NaBH₄ increased the decolorization of MB dye when it was utilized together with TiO₂/NiO bilayer photocatalyst. TiO₂/NiO bilayer photocatalyst leached 90 and 35 ppm of nickel cations into the CBR dye solution for the first treatment when illuminating under UV light and visible light. Leached nickel cation reduced in the following treatment to less than 10 ppm after 3rd treatment for both UV and visible light illumination system. There was no iron (III) cation was leached into the dye solution under visible light illumination. Nickel cation did catalyze decolorization of CBR dye solution but retarded the decolorization of MB dye when illuminating under visible light with the presence of TiO₂/NiO bilayer photocatalyst and aeration. Results from TEM, XRD, EDX and BET show that NiO that had been calcined at higher temperature has bigger particle size. Finally, TiO₂ photocatalytic activity could be enhanced by coupling with NiO and chitosan as second layer. However, the enhancement is mostly for anionic dye. Chitosan enhances TiO₂ photocatalytic activity more than NiO. Nickel ion that has leached from the NiO adsorbent does influence the photocatalytic activity of the TiO₂/NiO. All of the oxidants increase the decolorization of anionic dye but decrease the decolorization of cationic dye. Chitosan is more suitable and better adsorbent compared to NiO because it does not release any toxic contaminant into the treated solution. Whereas, NiO adsorbent

releases toxic nickel cation into the treated solution and further step is needed to remove the nickel cation.

CHAPTER ONE

INTRODUCTION AND LITERATURE REVIEW

1.0 Introduction

Water pollution is a major problem in the 21st century, especially in the developing countries. Now, people have realized that water is not an endless resource. Due to the global population growth, the need of clean water also grows. With the rapid development of science and technology, many industries, such as chemical, petrochemical, pharmaceutical and mining need huge amounts of water in their manufacturing processes. Ultrapure water is required in the pharmaceutical, microelectronics and semiconductor industries. Unfortunately, these industries have to discharge water, which is normally contaminated with toxic organic and inorganic compounds. In the recent two decades, water and air are contaminated to an unacceptable level all over the world by the pollutants coming from a variety of industrial and agricultural activities. Meanwhile, governments in most countries nowadays no longer tolerate untreated factory discharges and under the public pressure, regulations have been established to stipulate the level of contamination in the discharged water. Hence, innovative and effective water treatment processes are needed to treat the discharged water effectively in order to maintain the sufficient need of water resources.

The purpose of water purification is to reduce the pollution levels in discharged streams to meet the government regulations and to purify the water to ultrapure levels for industries involving pharmaceuticals, microelectronics and semiconductor. The ideal water treatment process should possess the ability to fully mineralize all the toxic species present in the waste stream without leaving any hazardous residues in the treated water. Besides that, it should be cost effective and economical. However, none of the available treatment technologies has achieved this ideal condition. There are a

number of waste disposal methods, which are currently applied with varying degrees of success. Figure 1.1 shows the various wastewater treatment technologies either currently available or at various stages of development.

Most of the industrial wastes are disposed based on the phase transfer principles processes (Conner, 1990), even though none of them is completely satisfactory. Air stripping is commonly used for removing volatile organic contaminants in wastewater. The process merely transfers the pollutants from the water phase to air phase without destroying them. Another commercialized process for water purification is granular activated carbon adsorption. In this case, the pollutants are transferred from the liquid phase into the solid phase. However, the spent carbon, which contains adsorbed pollutants, must then be disposed again. Because of the above reasons, alternative destructive oxidation processes for water treatment has been given greater attention (Matthews, 1992).

All of the above mentioned treatment methods are non-destructive technologies. Two available destructive technologies currently being used in the water industries are chlorination and ozonation. However, both chlorine and ozone are hazardous strong oxidants, which are not environmental friendly. Furthermore, ozonation has been proven to generate small levels of bromate ions, which are recognized as cancer causing agents (Mills and Hunte, 1997).

Biodegradation is another available destructive technology but its efficiency in degrading industrial waste water is low due to its very slow degradation rates. It is also known to present difficulties during operation at higher concentrations of organic contaminants (Pelizzetti *et al.*, 1990). In addition, active microorganisms that are intended to degrade organic contaminants may at times be killed by the toxicity of the organic contaminants present in the waste water. Therefore maintenance of these

micro-organisms at times can be very expensive. Incineration of organic wastes has been broadly used in developing countries. However, it releases toxic secondary pollutants into the air such as dioxin and furan (Shaub and Tsang, 1983).

In order to deal with the degenerating environment and to solve pollution problems from commercial wastewater discharges, researchers and scientists have been developing new innovative treatment processes. These processes are a new class of technologies that could be used promisingly to treat toxic organics in contaminated water. These new technologies are known as advanced oxidation processes (AOPs), which utilize H_2O_2 , O_3 , TiO_2 , vacuum and UV light. Major AOPs processes are $\text{H}_2\text{O}_2/\text{UV}$, O_3/UV , $\text{H}_2\text{O}_2/\text{O}_3/\text{UV}$, TiO_2/UV and VUV (see Figure 1.1).

In $\text{H}_2\text{O}_2/\text{UV}$, H_2O_2 undergoes homolytic dissociation into two hydroxyl radicals upon illumination by UV light (mainly at 254 nm). These highly reactive hydroxyl radicals will attack and decompose the organic compounds present in the solution. The mechanisms involved are hydrogen abstraction, electrophilic addition and electron transfer. Formation of the hydroxyl radicals in this process sets the limit of its oxidation rate of the contaminants. This is because the organic substrates act as inner filter to the UV light, which illuminates the substrate (Legrini, 1993).

Combination of ozone with UV light is another hydroxyl radical generating process. It can oxidize a great variety of organic compounds in the wastewater. In this process, aqueous systems that have been saturated with ozone, are irradiated with UV light at 254 nm. Oxidation-degradation rates in this process are much higher than the treatments carried out separately with either only ozone or UV light irradiation. The problem with this method is the low ozone solubility in the water and the limitations of the mass transfer in the photoreactor (Khan *et al.*, 1985). Addition of H_2O_2 into the

O_3/UV process could enhance the oxidation-degradation rate via photochemical generation of hydroxyl radicals.

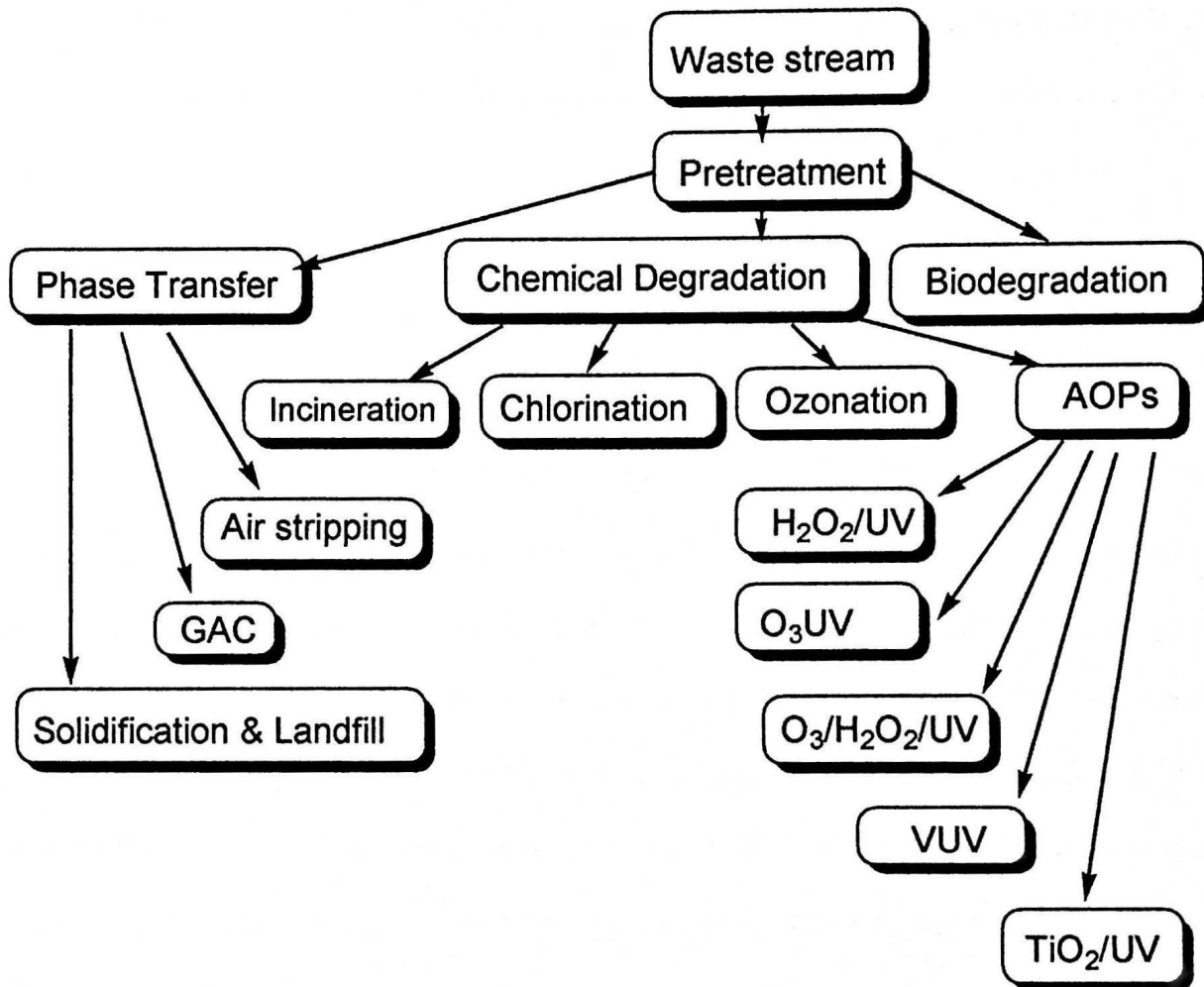
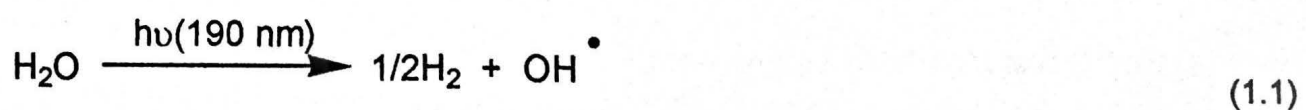


Figure 1.1: Various wastewater treatment technologies in environmental engineering (Chen *et al.*, 2000).

Note: GAC: Granular activated carbon; VUV: Vacuum ultraviolet; AOP: Advantage oxidation processes

The vacuum ultraviolet (VUV) process uses UV-C (wavelength from 100nm to 290nm) to dissociate the H_2O molecules to hydrogen and hydroxyl radicals. The proposed mechanism is shown in equation 1.1:



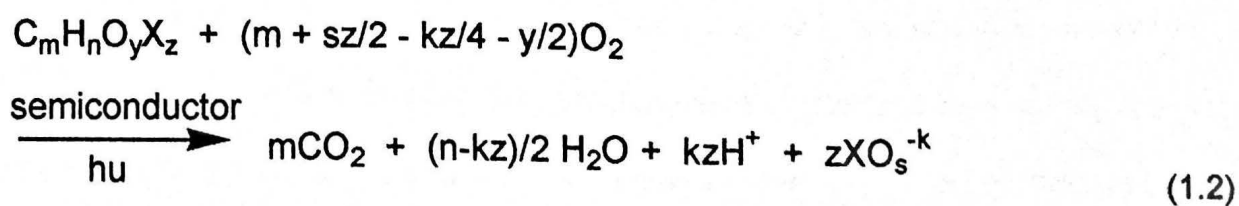
The UV-C light is produced from the excimer lamp at wavelength of 190 nm. This process is quite simple and has a distinct advantage whereby no chemicals are needed during the treatment of the wastewater. However, there are only a few research groups having this capability due to the limited availability of the excimer light sources (Legrini, 1993).

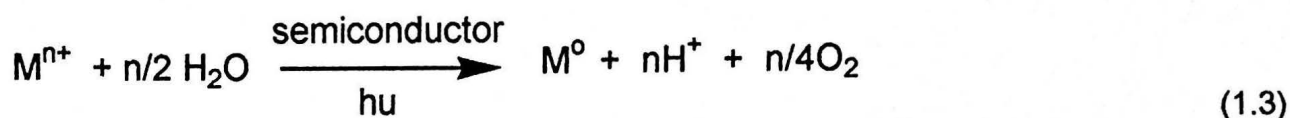
The main purpose of AOPs is to produce complete mineralization of organic compounds into carbon dioxide and mineral acids (Schiaello, 1988). Among the AOPs processes, heterogeneous photocatalysis (TiO_2/UV) has received a lot of attention in the last 20 years as an alternative method to treat water containing organic compounds and metal ions. This process is based on the photocatalytic property of the semiconductor to produce hydroxyl radicals under UV light irradiation. This technique has emerged as a feasible alternative to solve environmental problems and to overcome many of the drawbacks that exist in the traditional water treatment technologies. Heterogeneous photocatalysis is different from the other AOPs process because its photocatalyst is reusable and additional oxidants are unnecessary in this process. The main advantages of this technique are:

- (i) The oxidation is powerful enough to mineralize almost all-organic pollutants in wastewater and carbon tetrachloride (Choi *et al.*, 1994), which was considered as hydroxyl radical resistant (Ollis, 1985).
- (ii) It is considered as a green technology because the ultimate products are CO_2 and H_2O and mineral acids, which are harmless to the environment.
- (iii) The oxidant used in this process is atmospheric oxygen and therefore, it is unnecessary to add extra oxidizing agents.
- (iv) The catalysts are non-hazardous, chemically stable, reusable and inexpensive.
- (v) The catalysts can be activated using low energy UV-A light and therefore, solar illumination can be utilized.

- (vi) The process can remove large capacities of the intermediates; therefore, it is commercially comparable to activated carbon adsorption process (Ollis *et al.*, 1989; Miller and Fox, 1993).

Another innovative technology is photoelectrochemistry. This technology has been given a lot of attention because the irradiated TiO₂ electrodes in water could split water into hydrogen and oxygen. This finding was discovered by Fujishima and Honda in 1972 (Fujishima and Honda, 1972). Since that time, researchers also discovered that TiO₂ have the photocatalytic potential to oxidize organic compounds in water to carbon dioxide and mineral acids. The first study involving photocatalysis as a method for water purification was carried out by Pruden and Ollis. (1983). In their study, they discovered that TiO₂ was able to degrade trichloroethylene in water. They also studied the degradation of chloroform by photoassisted heterogeneous catalysis in dilute aqueous suspensions of TiO₂, heterogeneous photoassisted catalysis conversion of perchloroethylene, chloroform and carbon tetrachloride (Hsiao *et al.*, 1983), perchloroethylene, dichloroethane, chloroacetic acids and chlorobenzene (Ollis *et al.*, 1984) with illuminated TiO₂ photocatalyst. Since then, a variety of dissolved organic compounds, which could be oxidized to CO₂ by photocatalysis had been studied (Ollis, 1985). Besides oxidation of organic compounds, heterogeneous photocatalysis can also reduce some toxic metal ions such as silver (Hermann *et al.*, 1988), chromium (VI) (Kalil *et al.*, 1998), mercury (Serpone, *et al.*, 1987) and platinum (Angelidids *et al.*, 1998). The oxidation and reduction processes are given in equations 1.2 and 1.3:





1.1 Basic principles of heterogeneous photocatalysis

Photocatalysis refers to the combination of photochemistry and catalysis. Both light and catalyst have to be presented together in system in order for the chemical transformation could occur (Kisch, 1989). The catalysts are semiconductors, which can act as catalyst only when they are illuminated with light. This is due to the specific electronic structure characteristic of the catalyst involving an empty conduction band and filled valence band (Boer, 1990). The energy gap between the conduction band and the valence band is relatively small. The energy gap is called bandgap energy and its value usually in the order of a few electronvolts. The electron in the filled valence band can be promoted into the conduction band with a sufficient energy photon. Separation of this charge is an essential step of the photocatalytic reaction. This charge separation process is illustrated in Figure 1.2 and is represented in equation 1.4:



The excited electron in the partially filled conduction band and the vacancy in the partially filled valence band can move freely through the semiconductor lattice. The vacancy in the partially filled valence band is referred to as holes and is represented by h^+_{vb} . The reactions, which involve the photogenerated electron-hole pairs, are (a) recombination of the electrons and holes with liberation of the absorbed energy in the form of heat, and (b) reaction with electron donor or acceptor substances, which are added into the system to enhance the oxidation and reduction processes respectively.

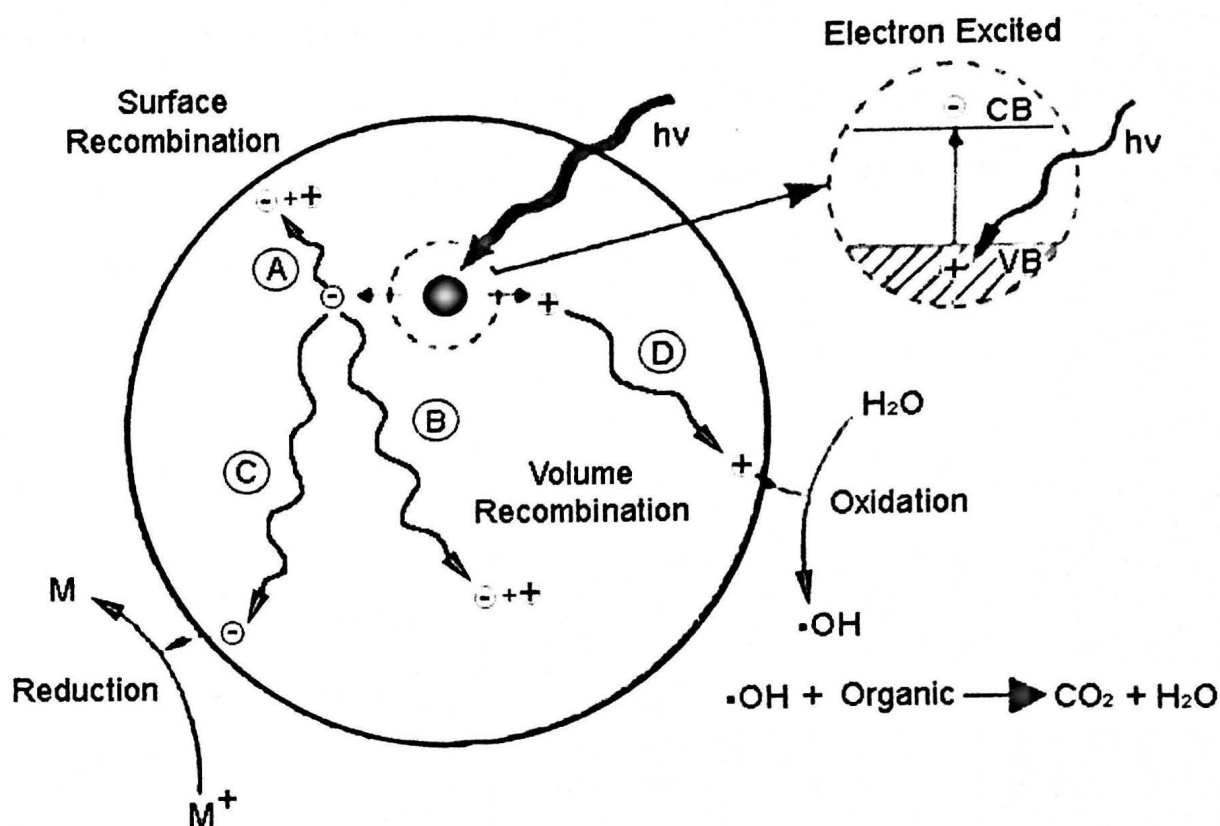


Figure 1.2: Illustration of the generation of electron hole pairs in a spherical semiconductor particle (Boer, 1990)

Valence and conductance band position of various semiconductors and relevant redox couples are illustrated in the Figure 1.3. The reaction pathway of the degradation process is determined by the position of the conduction and valence band of a semiconductor. As an example, MoS_2 with a bandgap of 1.8 eV can thermodynamically photooxidize water but $CdSe$ with a bandgap energy almost similar with MoS_2 is unable to photooxidize water thermodynamically. Instead, $CdSe$ can easily photoreduce water because its conduction band position is higher than MoS_2 . In order for a semiconductor particle to act as photocatalyst in the oxidation reaction, the redox potential of the photogenerated valence band hole must be positive enough to generate adsorbed hydroxyl radical, which is a powerful oxidant for oxidation of organic pollutants. In the other hand, in order for the semiconductor particle to act as photocatalyst in the reduction reaction, the redox potential of the photogenerated conduction band electron must be negative enough to reduce the adsorbed oxygen

into superoxide or to reduce the adsorbed metal ion into its metallic form. The number of photogenerated electron-hole pairs in the semiconductor particle is dependent on the intensity of the light that is used to irradiate the semiconductor particle and also on the electronic characteristics of the surrounding material or substances that are able to prevent the recombination of the electron-hole pairs

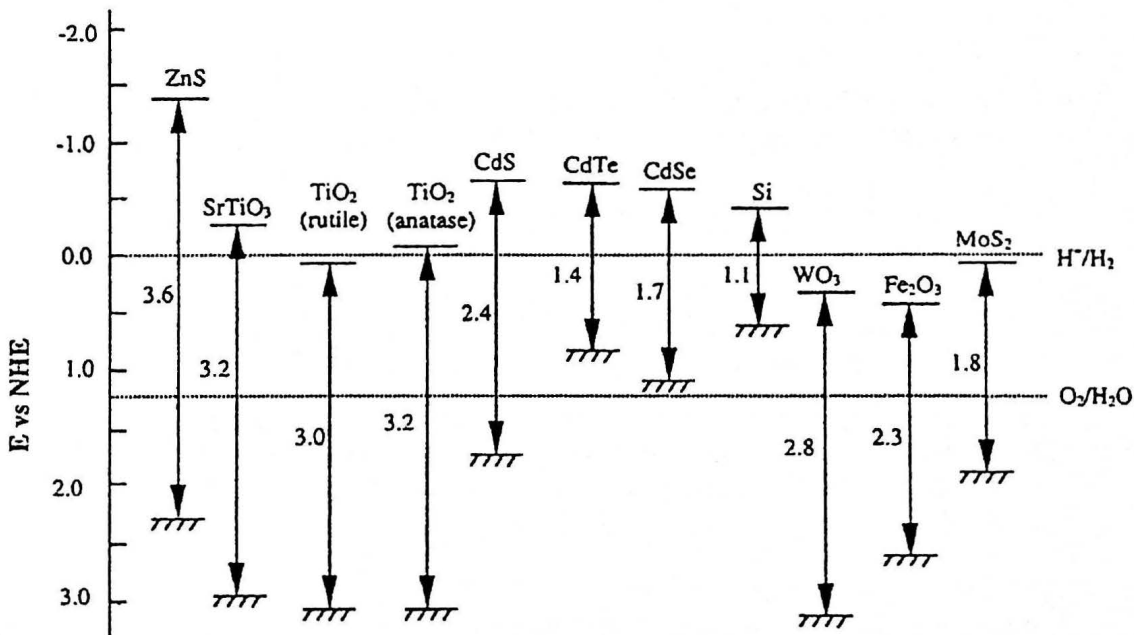


Figure 1.3: Valence and conduction band positions of semiconductors at pH = 0 (Suppan, 1994).

Hence, photocatalytic technology is different from other water treatment methods because it involves both oxidation and reduction reactions. Reduction reactions are mainly used to remove dissolved metal ions whereas the oxidation reactions are used to mineralize the dissolved toxic organic compounds. The oxidation and reduction processes must occur simultaneously in order for the overall photocatalytic activity to be sustained. In the photocatalytic process, organic compounds and water molecules act as reductants whereas oxygen and metal ion act as oxidants. Both oxidation and reduction kinetics are interdependent and either one can be a rate-controlling step to the whole process.

Semiconductor materials, which are commercially available and able to act as photocatalysts are TiO₂ (Augugliaro *et al.*, 1991), ZnO (Barbeni *et al.*, 1985), CdS, ZnS (Al-Sayyed *et al.*, 1991), Fe₂O₃ and WO₃ (Beknolet *et al.*, 1996). However, not all of them are suitable for catalyzing oxidation and reduction reactions for a wide range of organic compounds and inorganic compounds. Table 1.1 shows the photocatalytic semiconductors, which are commonly used in water treatment process.

Table 1.1: Bandgap energies of various semiconductors at pH = 0 and its corresponding threshold wavelength (Rajeshwar and Ibanez, 1997)

Semiconductor	Bandgap (eV)	Wavelength (nm)
TiO ₂	3.0-3.2	413-388
ZnO	3.2	388
ZnS	3.6	335
CdS	2.4	516
Fe ₂ O ₃	2.3	539
WO ₃	2.8	443

The threshold wavelength could be calculated using the following equation:

$$\lambda_{bg} \text{ (nm)} = 1240/E_{bg} \text{ (eV)} \quad (1.5)$$

However, threshold wavelengths, which are shown in the Table 1.1, may be altered when the semiconductor surface is in contact with the electrolyte solution (Finklea, 1993). Lower bandgap energy semiconductors are preferred for photocatalytic activity when solar energy is used for the activation. However, low bandgap semiconductors such as CDS and CdSe are unstable (Mills and Morris, 1993) and its ions are easily leached into the water.

An ideal photocatalyst must have high activity, ability to be activated with visible or near UV light energy, stable when irradiated under light, reusable, chemically and

biologically inert and inexpensive. Among the semiconductor photocatalysts, which have been tested in laboratory studies, TiO_2 is the most popular and is extensively used in both laboratory studies and pilot plants (Hermann *et al.*, 1983). Moreover, sunlight that contains about 3% of UV-A ($\lambda \leq 388\text{nm}$) can be used as light source to activate TiO_2 (Turchi *et al.*, 1993).

Titanium dioxide exists in two crystalline forms i.e. anatase and rutile. In most studies, anatase has been proven to oxidize acid/acetate mixtures (Krautler and Nard, 1978), phenols (Sclafani and Hermann, 1996), cyclohexane and 2-propanol (Sclafani and Hermann, 1996) and was always more effective than the rutile form. Anatase form has a well-defined nature, is non porous with BET surface area of $554 \pm 15 \text{ m}^2/\text{g}$ and has an average particle size of 30 nm (Chen *et al.*, 2000). Its photocatalytic activity is higher than most other available crystalline forms of TiO_2 .

1.2 Mechanism of the Photocatalytic Reaction

Although the overall reactions of the photocatalytic semiconductor are oxidation and reduction, the main steps that cause both oxidation and reduction are still not well understood. The photocatalytic process is a four-phase system, which consists of electronic phase, liquid, solid and gas phases. The electronic phase is the UV light source. It relates to the excitation of the electron in the valence band into the conduction band. The liquid phase is the wastewater, solid phase is the catalyst and the gas phase is the oxygen that is contained in the water. When a semiconductor particle is illuminated by light that has higher energy than the semiconductor bandgap energy, E_{bg} , electrons, which occupy the valence band, will be excited to the conduction band. Subsequently, a hole is generated in the valence band and the free electrons are produced in the conduction band (Equation 1.4). This reaction is the first essential step of the photocatalytic reaction. Since the catalyst is always in contact with the liquid solution, transfer of the charge would occur until it has achieved an

electrostatic equilibrium. In metals, excessive charge is confined on the surface. However, in the semiconductor, the excessive charge would be distributed in a region, which is called space-charge region. Existence of this region is due to the expansion of this region from the surface to the bulk of the semiconductor. This region plays a very important role in the photocatalytic process. Due to the presence of the surface charge region, the photo-excited electron can be separated from the hole and migrate (k_{diff}^{e-} , k_{diff}^{h+}) to the particle surface. This would produce a potential gradient between the bulk solid and its external surface. This potential gradient is caused by the depletion of the conduction band electrons in the space charge-region (Bard, 1979). Electro-neutrality of the surface can only be formed when the electrons and holes have equal arrival rates at the steady state condition (Childs and Ollis, 1981). Equations 1.6 and 1.7 represent the electron-hole pairs migration.



The fate and the dynamics of the photogenerated electron-hole pairs are very important in the degradation processes. Commonly, photogenerated electrons and holes have two basic destinies. The first one is the recombination of the photo-excited electron with the holes and the input energy is released as heat. This may happen during their transportation to the particle surface (Equation 1.6). Besides that, they may react with the electron acceptor and electron donor, which accumulate on the particle surface after they have migrated to the catalyst surface. Consequently, they initiate the reduction and oxidation processes, which are represented by equations (1.9) and (1.10)



Where, A is the electron acceptor and D is the electron donor.

Reaction in equation (1.8) is mainly caused by the low efficiencies of photocatalytic processes and according to Alfano *et al.* (1997), the recombination (k_{rec}) of the electrons and holes occurs mainly in the bulk of the catalyst particle. The possibility of this recombination can be prevented if the separated mobile species are trapped by surface adsorbates or other sites. If the surface adsorbates possess a redox potential, which is appropriate for a thermodynamically allowed reaction, the photogenerated hole that has reached the surface may have high probability to react with the surface adsorbates. Hence, a hole can oxidize (k_{ox}) the adsorbed electron donor by abstracting the electron from it while the mobile free electron in the conduction band can reduce (k_{red}) the adsorbed acceptor by transferring the electron to it. After the electron donor has been oxidized, it would become a cation radical and the electron acceptor, which has received electron from the conduction band, would become anion radical. These radical ions can take part in several reaction pathways. The first pathway is reacting chemically with themselves or other adsorbates. The second is combining by back electron transfer to form an excited state of one of the reactants or to waste the excitation energy by the non-radiative pathway. The third is diffusing from the semiconductor surface and reacting chemically with other species in the bulk solution. If the rate of the formation of cation radical is almost similar to the rate of the back electron transfer, any molecule with an oxidation potential less positive than the semiconductor valence band edge would be oxidized through a photoinduced

process. This is because under these conditions, interfacial electron transfer at the illuminated interface is thermodynamically possible. Similarly, the reduction, which is induced by photons, can also occur to any molecule possessing a reduction potential, which is less negative than the conduction band edge (Fox. and Dulay, 1993).

TiO₂ surface is readily hydroxylated when it is in contact with water. Water and dissociated water molecules are bonded to the TiO₂ surface. The hydroxylated surface coverage of 7 – 10 OH⁻/nm² at room temperature had been reported by Morishige *et al.* (1985) and Suda and Morimoto (1987). Turchi and Ollis (1990), Jaeger and Bard (1979) and Fox and Chen (1981) had experimentally observed the reactions of the trapped holes with adsorbed solvent molecules (H₂O and OH⁻). They concluded that hydroxyl radicals were produced when the holes that migrated to the semiconductor surface abstracted electron from the water molecule or hydroxyl ion. Equations (1.11) and (1.12) are used to represent these reactions;



Where, ads means adsorption.

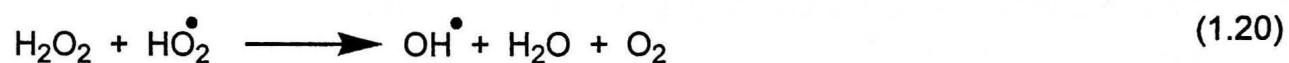
Besides that, these holes can also abstract electron from the adsorbed organic substrates RX according to equation 1.13:



Due to the high concentration of adsorbed H₂O and OH⁻ on the catalyst particle surface, the reactions, which are more important in the oxidative processes, are equations (1.11) and (1.12). Manthews (1984) had studied the oxidation process in

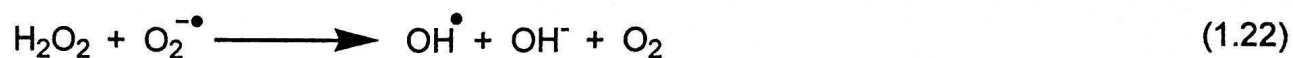
water-free aerated organic solvents and discovered that only partial oxidation can be achieved. However, complete mineralization of numerous organic compounds in aqueous solutions has been reported by Al-Ekabi *et al.* (1989), Matthews, (1990), and Low *et al.*, (1991). According to Low *et al.*, (1991), the nitrate and ammonium ions were formed in titanium dioxide mediated photocatalytic degradation of organic compounds containing nitrogen atoms. This proved that organic compounds have been totally mineralized to carbon dioxide, water, mineral acid and ion. Based on the above reports, it is obvious that direct reaction between the organic compounds and the valence band holes (Equation 1.13) is insignificant (Wang *et al.*, 1992). Therefore, in order for the organic compounds to be completely destroyed, the presence of water and hydroxyl groups are necessary. Photogenerated electrons must also react in order for it not to accumulate in the catalyst particles. Accumulation of the photogenerated electrons on TiO₂ particles had been reported by Wang *et al.* (1992) when TiO₂ was used to oxidize 1.6M aqueous methanol.

The hole consumption rate must be equal to the electron consumption rate when the photoassisted reaction is at the steady state. Therefore, electron scavengers or acceptors, which are used to trap the excess electrons, must be present in the photocatalytic process. The most common electron acceptor, which is available at little or no cost is oxygen. The reactions between oxygen and the electron at the surface of semiconductor had been discussed by Okamoto *et al.* (1985a), Krautler and Nard (1978), Matthews (1984) and Al-Ekabi and Serpone (1988). The reactions are represented in equations (1.14) and (1.20) are as follows:



Jaeger and Bard (1979) had verified the formation of these species using electron spin resonance measurements. Formation of H_2O_2 in the degradation of phenol in TiO_2 suspensions by aerating the solution with O_2 and He, respectively also has been confirmed by Auguliario *et al.* (1990). Species, which are generated from equations (1.14) to (1.20), are present either at the interface or in the solution and can take part in the complex degradation scheme and will finally leads to the final mineralization of organic species. Through this complex degradation scheme, one hydroxyl radical is generated from three electrons. In the other half-cell reaction, one hole produces one hydroxyl radical (Equations 1.10 and 1.11). Therefore, most of the hydroxyl radicals are generated through hole reactions (Okamoto *et al.*, 1985b).

More hydroxyl radicals would be produced when the hydrogen peroxide formed from the reactions (1.16) and (1.19) decompose further through the following equations as depicted in equations (1.21) to (1.23):



Studies by Tanaka *et al.* (1989b), Wei *et al.* (1990) and Martyanov *et al.* (1997) showed that addition of hydrogen peroxide would improve the photocatalytic process. The improvement of the process would most probably be due to the reactions from equations (1.21) to (1.23). Turchi and Ollis. (1990), Bard (1979) and Matthews (1984) had proposed that the highly reactive hydroxyl radicals, which are formed from the above equations, are the primary oxidizing species in the photocatalytic processes and the rate determining reaction step may be the formation of hydroxyl radicals. This proposal is supported by the following facts:

- (a) Organic compounds cannot be completely mineralized in the water-free organic solvents (Matthews, 1984).
- (b) Concentration of the steady-state hydroxyl radicals in the UV-irradiated titanium dioxide aqueous solution could go to as high as 10^{-9} M (Ireland and Valinieks, 1992). This amount is much higher than those in the processes of ozonation, direct photolysis of H_2O_2 and radiolysis (i.e., $< 10^{-12}$ M)
- (c) The intermediates, which are detected during the photocatalytic degradation of aromatic mostly, have hydroxylated structures. These had been reported by Turchi and Ollis (1990), Okamoto *et al.* (1985a) and Augugliaro *et al.* (1988). The intermediates, which are produced in this reaction, are consistent with those found when the similar aromatics compounds are reacted with a known source of hydroxyl radicals (Cox, *et al.*, 1980).

Hydroxyl radicals are very reactive species. This is because it has an unpaired electron, which is highly unstable. It reacts rapidly and non-selectively with the organic

compounds through an oxidation pathway. It is able to oxidize almost all organic pollutants in the wastewater by abstracting the hydrogen from the organic compounds. This is due to its high oxidation potential (Table 1.2). The oxidation of organic compounds by the reactive hydroxyl radicals may take place either in the bulk solution or on the catalyst surface. Turchi and Ollis (1990) had proposed four different reaction pathways based on the reaction of the hydroxyl radicals with the organic compounds in the photocatalytic degradation process. These four reaction pathways are shown in equations (1.24) to (1.27) as follows:

(a) Reaction of the adsorbed hydroxyl radicals with the adsorbed organic species.



(b) Reaction of the non-bound hydroxyl radicals with the adsorbed organic species



(c) Reaction of the adsorbed hydroxyl radicals with a free organic species arriving at the catalyst surface



(d) Reaction occurs between two free species in the bulk solution.



Based on the different reaction pathways, four kinetic models had been developed, which had similar degradation rate forms and were consistent to the reported initial data and temporal degradation data. However, Fox (1993) reported that surface-bound hydroxyl radicals are more stable compared to those in the bulk solution when pulse radiolysis and time-resolved diffusion reflectance was used to measure the

hydroxyl radicals concentration in the photocatalytic process. Minero *et al.* (1992) had obtained similar results indicating that the degradation process occurs at the surface or within a few monolayers around the photocatalytic particles. All of these results show that the main reaction of the photocatalytic degradation process occurs on the surface of the catalyst.

Peroxy radicals in equations (1.24) to (1.27) are added to the oxygen molecules and initiate thermal (chain) reactions leading to the formation of CO₂, H₂O and mineral acid according to equation (1.28):

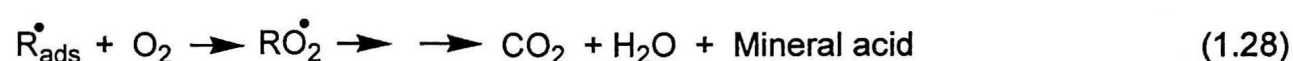


Table 1.2: oxidation potentials of some oxidants (Legrini, *et al.*, 1993)

Species	Oxidation Potential (V)
Fluorine	3.03
Hydroxyl radical	2.8
atomic oxygen	2.42
ozone	2.07
hydrogen peroxide	1.78
perhydroxyl radical	1.7
permanganate	1.68
hypobromous acid	1.59
chlorine dioxide	1.57
hypochlorous acid	1.49
hypoiodous acid	1.45
chlorine	1.36
bromine	1.09
iodine	0.54

Superoxide and /or perhydroxyl radicals, which are formed from the reduction of the oxygen by the catalyst during photocatalytic oxidation of organic compounds, eventually form hydroxyl radicals that enter into the oxidation cycle (Mills and Hunte, 1997). Besides oxygen, any dissolved metal ions can consume electrons and complete the redox cycle as long as the reduction potential of the metal ions are more positive than the conduction of the photocatalyst. After the metal ions have been reduced, the

reduced form of metal usually deposits on the catalyst surface, which may or may not be easily removed (Foster *et al.*, 1993). The positions of the valence and conduction bands of anatase TiO₂ photocatalyst in contact with an aqueous electrolyte solution at different pH and reduction potentials of some of the environmentally fretful metal ions were shown in the Figure 1.4. The position of both conduction and valence bands of anatase TiO₂ are pH dependent. The positions of these bands may shift to more cathodic potentials when the pH of the electrolyte of the solution is increased (Chen *et al.*, 2000). However, reduction potentials of all metal ions except Cr (VI), which are shown in Figure 1.4 are not dependent on pH. Therefore, these would mean that the metal ions are more favorable to be photo-reduced with increasing of pH.

Based on the information in Figure 1.4, Cd²⁺, Fe²⁺ and Cr³⁺ cannot be photo-reduced by TiO₂ because their reduction potentials are more negative than that of photo-excited electrons in the TiO₂. However, Au³⁺, Cr⁶⁺, Hg²⁺ (including HgCl₂, HgCl₄²⁻), Ag⁺, Hg₂²⁺, Fe³⁺, Cu⁺ and Cu²⁺ can be reduced thermodynamically. Among the above metal ions, Fe³⁺ and Cr⁶⁺ could not be reduced to iron and chromium metals respectively but they could be reduced to Fe²⁺ and Cr³⁺. For Pb²⁺ and Ni²⁺, due to their low driving force, it is also unlikely to be reduced under most conditions. Moreover, concentration of the particular metal ion may alter its redox reduction potential. Besides, according to Figure 1.4, oxygen is expected to be reduced preferentially compared to most ions if it is present in the solution. That is the reason why nitrogen gas is used to purge the reaction system in most studies. The purging is to eliminate the oxygen gas and to increase the photo-reduction efficiency of the metal ions.

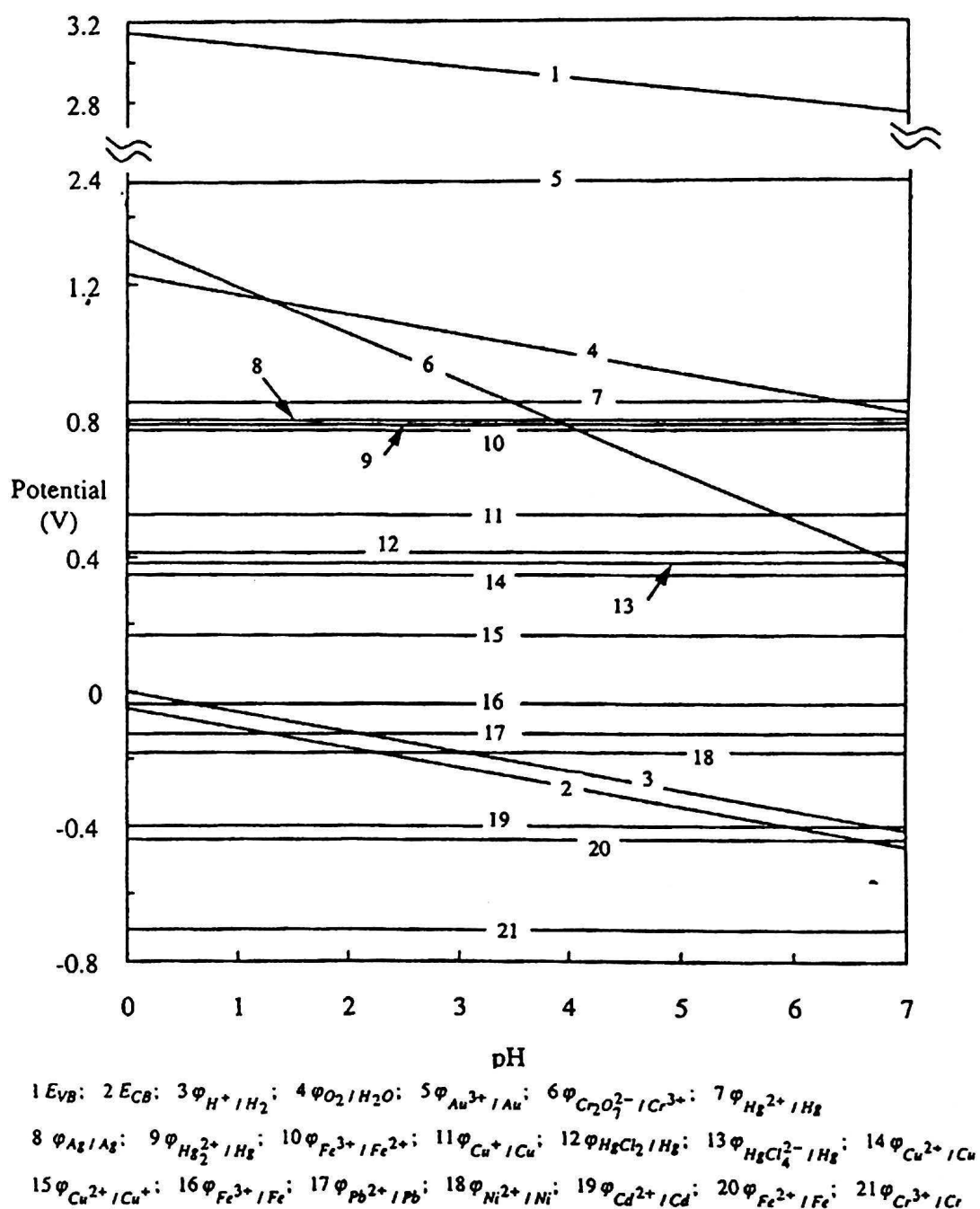


Figure 1.4: Positions of valence and conduction bands of TiO_2 (anatase) and the reduction potentials of metallic ions of interest at different pH (Chen *et al.*, 2000).

1.3 Role of adsorption in photocatalytic degradation

The role of adsorption in photocatalytic degradation is very important in order to determine the rate of the whole degradation process. This is because when the targeted organic contaminant to be degraded moves slowly toward the photocatalyst surface, less organic contaminant would be degraded within a certain period of time, no matter how good the photocatalytic potential that is possessed by the photocatalyst.

Therefore, adsorption of the organic contaminant by the photocatalyst is the determining step that has to be taken into account in order for the whole degradation process could be optimized. Organic contaminants that adsorb faster onto the photocatalyst surface can increase the degradation rate. However, organic contaminants, such as dyes that adsorb too fast onto the photocatalyst surface will show a very promising decolorizing treatment during the first run but quite poor performance in the following treatment. This is due to the excessive organic contaminants that is adsorbed onto the photocatalyst surface and prevent the light from reaching it. Once the photocatalyst does not receive the light energy to excite its electron from the valence band to conduction band, there would be no generation of holes and the usual photocatalytic mechanisms would not proceed on the photocatalyst surface.

Concerning the effect of adsorption during the photocatalytic degradation of pollutants, Bekkouche *et al.*, (2004) had studied the adsorption of phenol on titanium dioxide (TiO₂) in suspension form. The experiment was carried out by mixing the phenol solution with the suspended titanium dioxide mixture and the system's temperature was maintained at 25 °C. Sample was collected at regular intervals by syringe and filtered before measuring it using UV-vis spectrophotometer. The equilibrium of adsorption was reached after one hour of stirring. The conclusion that had been drawn was that phenol was weakly adsorbed onto titanium dioxide. The type of adsorption between the phenol and titanium dioxide is chemisorption and it is represented well by the Langmuir model. The optimum pH range for this adsorption was between 5 and 6. This study also showed that there was an advantage to operate the adsorption at great velocity of agitation by ultrasonic drives and also at natural pH. Ultrasonic agitation increased the quantity of phenol adsorbed by 5 %. This mode of agitation reduces the phenomenon of agglomeration of titanium dioxide particles and therefore increases the interfacial area of the catalyst.

The kinetics of photocatalytic degradation of four different model organic compounds namely formic acid (FA), oxalic acid (OA), 4-chlorophenol (4-CP) and the herbicide monuron (3-(4-chlorophenyl)-1,1-dimethylurea) in a self-constructed batch-mode plate photoreactor with a thin flow of contaminated aqueous solution circulating over an illuminated particulate layer of P25 TiO₂ (Degussa) had been studied by Kry'sa *et al.*, (2006). Both OA and FA were found to be adsorbed on TiO₂ surface. Their mineralization, induced by direct transfer of photogenerated holes, proceeded in a single step, without observable intermediates, following approximately zero order kinetics. Numerical simulations were performed using a newly proposed kinetic model based on the photostationary state assumption. The model allowed an explanation of the order of the observed reaction as well as independent comparison between competitive adsorption of organic compounds and oxygen on the photocatalyst surface thus yielding a better fit for the case of competing 4-CP and monuron. These two organic compounds were not adsorbed by the photocatalyst under the conditions used and were degraded through the action of photogenerated hydroxyl radicals. Most important, it was concluded that their degradation proceeded with lower photoefficiency than for the adsorbed compounds (FA and OA). The mineralization of both 4-CP and monuron followed zero order kinetics and their degradation was close to first order. The different rates of reaction orders were consistently explained using the photostationary state approach. In this study, organic contaminants that were adsorbed onto the TiO₂ were degraded faster than the one that was not adsorbed by TiO₂. This is because the adsorption of the organic contaminants onto the TiO₂ particulate surface is the rate determining step within the degradation mechanism and therefore it affects the kinetics of the degradation process.

Shona *et al.*, (2005) had studied the effects of chemical coupling of flocculation and adsorption with photocatalysis in treating persistent organic pollutants in

wastewater. The experiment was carried out in suspension form and the results showed that initial reverse reaction occurred when titanium dioxide alone was used as a catalyst in the treatment. The results also showed that powdered activated carbon adsorption followed by photocatalysis were ineffective in alleviating reverse reaction. However, when powdered activated carbon and titanium dioxide catalyst were added simultaneously in the wastewater, the reverse reaction was eliminated thoroughly.

Inumaru *et al.*, (2004) had prepared n-Octyl-grafted TiO_2 ($\text{C}_8\text{-TiO}_2$) as a model of a photocatalyst with high molecular adsorption selectivity. Photocatalytic activity of the model photocatalyst was investigated. They found out that the catalyst was highly active in the presence of concentrated phenol (1000ppm) and 4-nonylphenol (2ppm) and it decomposed both chemicals in 180 minutes, while pristine TiO_2 (P-25) under the same conditions showed much lower activity. The high $\text{C}_8\text{-TiO}_2$ activity was ascribed to the molecular selective adsorption of the organic molecules on the alkyl-grafted hydrophobic surface. Infrared spectra showed that the grafted alkyl groups were gradually decomposed under photoirradiation. The model catalyst demonstrated that molecular selective adsorption is important for removal of low-concentration contaminants in the presence of other, more concentrated compounds.

Franch *et al.*, (2005) had studied the role of Fe (III) on the TiO_2 -assisted photocatalytic degradation of maleic acid. The study on the kinetics of the removal of organic matter, as well as the identification of all the stable mineralization intermediates, demonstrated that the presence of Fe (III), adsorbed onto the TiO_2 surface, rendered a more efficient process through a cleaner mineralization pathway compared to bare TiO_2 . Furthermore, the behaviour of the system did not depend on the iron source. On the other hand, the influence of Fe (III) on the interaction of maleic acid with TiO_2 in the solid phase was studied using ATR-FTIR technique. In the TiO_2 + UV assays, maleic, acrylic, malonic, oxalic, acetic and formic acids have been